Scripta Materialia 120 (2016) 98–102

Contents lists available at ScienceDirect

Scripta Materialia

journal homepage: www.elsevier.com/locate/scriptamat

Regular Article

Influence of carbon content on the primary solidification mode of high strength steels in resistance spot welding conditions

Florent Krajcarz [a,b,1], A.-F. Gourgues-Lorenzon [b,*], E. Lucas [a]

[a] ArcelorMittal Global R&D, BP 30320, 57283, Maizières-lès-Metz cedex, France
[b] MINES ParisTech, PSL Research University, Centre des Matériaux, UMR CNRS 7633, BP 87, 91003 Evry cedex, France

ARTICLE INFO

Article history:
Received 12 February 2016
Received in revised form 7 April 2016
Accepted 8 April 2016
Available online xxxx

Keywords:
Advanced high strength steels
Welding
Solidification microstructure
Rapid solidification
Thermokinetic modelling

ABSTRACT

The primary solidification mode of resistance spot welds made of advanced high strength steels has been investigated as a function of carbon content. Electron backscatter diffraction and dendrite morphology analysis showed for the first time a transition from primary solidification into δ-ferrite (C ≤ 0.22 wt%) to primary solidification into austenite (C ≥ 0.29 wt%) with increasing carbon content. The description of this transition by using the so-called "interface response function" model is not fully satisfactory and strongly depends on input model parameters. Epitaxial growth from the heat-affected zone or from the slowly solidified zone could influence the solidification path.

Resistance spot welding (RSW) of low carbon advanced high strength steels may, for particular steel chemistries and welding conditions, involve sensitivity of the weld nugget to interfacial fracture. Ductile fracture starting from interdendritic sulphur- or phosphorus-rich particles [1,2], as well as brittle cleavage or intergranular/interdendritic fracture [3,4] could originate from solidification-induced segregations. These are stronger when solidification occurs into γ-austenite instead of δ-ferrite [5,6]. RSW of automotive steel sheets involves high values of solidification rate, $V > 10^{-3}$ m·s^{-1} and of thermal gradient, G, up to 1.5×10^{6} K·m^{-1}, leading to $GV > 10^{3}$ K·s^{-1} [7,8]. The primary solidification phase, yet being an important parameter to control the final microstructure and fracture properties of the nugget, is still poorly known.

The influence of carbon content on the critical amount of phosphorus and sulphur required to induce hot cracking during welding [9] might be related to its influence on the solidification sequence of iron alloys. Low carbon Mn-Si steels primary solidify into δ-ferrite in conditions close to equilibrium. However, under high solidification rates ($0.5–1 \times 10^{-2}$ m·s^{-1}) and high cooling rate (1.5×10^{3} K·s^{-1}), in situ time-resolved X-ray diffraction [10] evidenced primary solidification into γ-austenite for a 0.50Mn-0.234C-0.28Si-1.70Al steel. The so-called "interface response function" model [11] predicted primary solidification into ferrite for this steel chemistry, but into austenite for binary Fe-0.234C alloy under similar conditions. This contradiction with experiment was attributed to a lack in thermodynamic data on ternary interactions between C, Al and Fe. A peritectic transition has been reported from real-time measurements of a C-Mn-Al steel during tungsten inert gas (TIG) welding [12]. A transition in solidification sequence with increasing cooling rate was evidenced for a 0.38C tool steels under TIG welding [13]. Nevertheless, the geometrical constraints associated to RSW render in situ diffraction measurements difficult. To the authors' knowledge, no such results have been reported up to now for RSW of low carbon steels.

The present study aims at determining the influence of carbon on the primary solidification mode of model high-strength steels under RSW conditions and at assessing whether local solidification conditions (as estimated using the interface response function model) might explain that influence, at least far from the fusion boundary. For this purpose, Fe-C-1.9Mn-0.21 Si-0.001S-(0.01 to 0.02)P (wt%) chemistries were chosen with a carbon content of respectively 0.153 (C153), 0.220 (C220), and 0.290 wt% (C290). As in [1], 2-mm-thick bare sheets were spot welded with a low welding current, without cold times (i.e., the AC current was continuously applied all along the welding time), leading to a weld diameter of 6 mm. The microstructure of base metal was predominantly ferritic. Preliminary finite element calculations with Sorpas dedicated software [14] showed slow solidification before current shutdown (i.e. during the welding time) followed by rapid solidification during the so-called holding time: $GV \approx 2 \times 10^{3}$ K·s^{-1}, $G \approx 0.86–6.1 \times 10^{5}$ K·m^{-1} and $V \approx 0.39–5.7 \times 10^{-2}$ m·s^{-1}. Thus, these calculations showed increasing values of V during the holding time. Close to the fusion boundary, a slowly solidified region was produced by alternating partial remelting and partial solidification during the end of the welding

* Corresponding author.
E-mail address: anne-francoise.gourgues@mines-paristech.fr (A.-F. Gourgues-Lorenzon).
[1] Present address: Aperam Isbergues research center, BP15, 62330 Isbergues, France.

http://dx.doi.org/10.1016/j.scriptamat.2016.04.011
1359-6462/

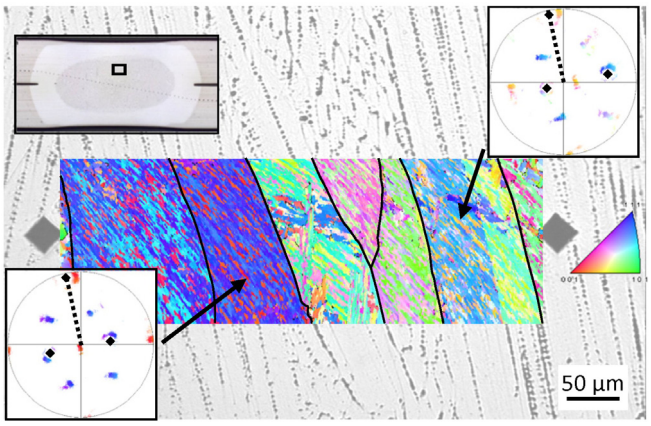

Fig. 1. C290 weld nugget: analysis of the region located in the black box in the upper left inlet macrograph. The inverse pole figure map (colour coded according to the sample normal, austenite grain boundaries highlighted in black) is superimposed to the LOM. {100} pole figures of martensite (colour dots) and of austenite (full diamonds) compare dendrite growth direction (thin black dotted line) with $<100>_{\gamma}$. (For interpretation of the references to color in this figure legend, the reader is referred to the web version of this article.)

time, when heat produced by the Joule effect was partly compensated by heat extraction from the water-cooled electrodes. The longer the welding time, the thicker this region [15]. During this transient, slow solidification stage, strong segregation occurred in the form of bands parallel to the planar solidification front and the values of G and V could not be accurately determined. Moreover, the microstructure of the heat-affected zone (HAZ) at the beginning of solidification could not be determined as e.g. in [16]. As a consequence, only the columnar-dendritic region that solidified during the holding time, far from the slowly solidified region was considered in the present work.

Metallographic cross-sections passing through the centre of the nuggets were polished and etched with Béchet-Beaujard reagent. Consistently with predictions using the criterion from Tiller et al. [17], columnar-dendritic solidification prevailed. Primary (λ_p) and secondary (λ_s) dendrite arm spacings were determined from light optical microscopy (LOM) using a linear intercept method. Whatever the steel chemistry, $\lambda_p \approx 9$–13 μm and $\lambda_s \approx 4$–5 μm. These values are constant, consistently with the constant value of GV and close [18] to predictions from Kurz-Fisher models [19,20], but too low for easy determination of solidification sequences from chemical gradients across dendrite arms. A simple alternative method was chosen, by considering that dendritic solidification into ferrite or austenite occurs along their <100> crystal directions even during rapid solidification [21,22]. After primary solidification into austenite, $<100>_{\gamma}$ keep parallel to dendrite growth directions. After primary solidification into δ-ferrite followed by transformation into austenite, $<100>_{\gamma}$ directions are generally strongly misoriented with respect to dendrite growth directions. By comparing dendrite growth directions and $<100>_{\gamma}$ directions, it becomes thus possible to identify the first phase to solidify in these regions.

Austenite grain morphology and crystal orientation were deduced from electron backscatter diffraction (EBSD) maps after a colloidal silica finish. Operating parameters were: high voltage 20 kV, tilt angle 70°, working distance 22 mm, hexagonal grid, step size ≈ 1 μm. 0.1×0.5 mm^2 columnar-dendritic regions were selected. The crystal orientation and morphology of parent austenite grains were deduced from $\{100\}_{\alpha'}$ poles figures of α′-martensite as in [23]. The corresponding dendrite morphology was determined with LOM. In the selected regions, dendrites were parallel to the cross-section plane, started from close to the slowly solidified region and appeared to have achieved steady-state growth.

For the C290 steel, up to 100-μm-wide parent austenite grains, elongated along the radial direction of the nugget, were readily determined from EBSD (Fig. 1). Their boundaries coincide with changes in dendrite morphology. From Fig. 1, the main dendrite growth direction, readily determined in five grains, was parallel to the radial direction of the nugget. Strong convection in the liquid [24] apparently did not interact with dendritic solidification; it was thus neglected in the following. The direction of primary trunks well agrees with the centre of one Bain zone of martensite, thus, with one $<100>_{\gamma}$ direction. These findings strongly suggest that primary solidification occurred there into austenite.

For the C153 steel, parent austenite grains were narrower (<50 μm), dendrites were more strongly entangled and groups of dendrites of similar morphology generally contained several parent austenite grains. In none of the eight investigated parent austenite grains was any $<100>_{\gamma}$ close to the dendrite growth directions (Fig. 2). Instead, one set of $<100>_{\alpha'}$ was close to the main dendrite growth direction. By taking orientation relationships between δ-ferrite and austenite, and between austenite and martensite into account, this suggests that solidification did not occur into austenite but into δ-ferrite.

The C220 steel chemistry yielded easier identification of dendrite morphology and also showed primary solidification into δ-ferrite (Fig. 3). Consequently, for the considered chemistries and welding parameters, a transition in primary solidification phase occurs for carbon content between 0.22 and 0.29 wt%. All these results are consistent with [10], yet with different steel chemistry and welding process but also under rapid solidification. Such a transition could contribute to the higher sensitivity of higher carbon bearing weld nuggets to brittle fracture induced by segregation of sulphur and phosphorus.

Equilibrium ThermoCalc calculations using the TCFe5 database predicted primary solidification into ferrite for the three chemistries, in contradiction with experiments. The thermokinetic "interface response function" model [11,25–28] was then used to describe the influence of steel chemistry on primary solidification into any phase φ under RSW

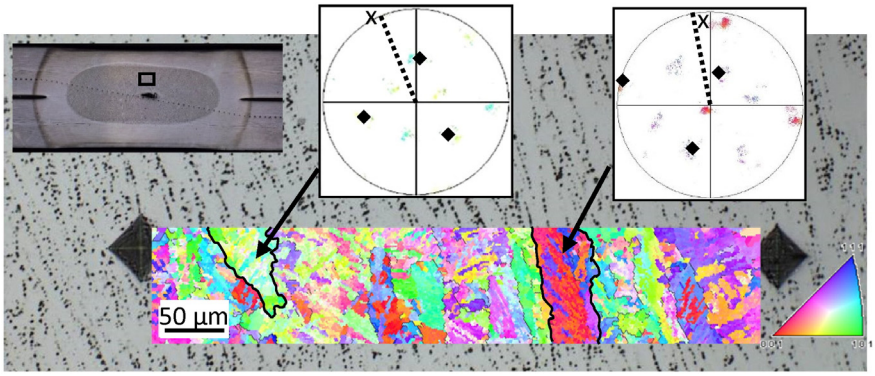

Fig. 2. C153 weld nugget: analysis of the region located in the black box in the inlet macrograph. The inverse pole figure map is superimposed to the LOM. Same colour and symbol coding as in Fig. 1. $<100>_{\alpha'}$ closest to the dendrite growth direction are indicated with a cross (X).(For interpretation of the references to color in this figure legend, the reader is referred to the web version of this article.)